CrossMark

J. Fluid Mech. (2020), *vol*. 901, R5, doi:10.1017/jfm.2020.541



Onset of three-dimensionality in rapidly rotating turbulent flows

Kannabiran Seshasayanan[1],† **and Basile Gallet**[1]

[1]Service de Physique de l'État Condensé, CEA, CNRS UMR 3680, Université Paris-Saclay, CEA Saclay, 91191 Gif-sur-Yvette, France

(Received 12 February 2020; revised 17 June 2020; accepted 30 June 2020)

Turbulent flows driven by a vertically invariant body force were proven to become exactly two-dimensional (2-D) above a critical rotation rate, using upper bound theory. This transition in dimensionality of a turbulent flow has key consequences for the energy dissipation rate. However, its location in parameter space is not provided by the bounding procedure. To determine this precise threshold between exactly two-dimensional and partially three-dimensional (3-D) flows, we perform a linear stability analysis over a fully turbulent 2-D base state. This requires integrating numerically a quasi-2-D set of equations over thousands of turnover times, to accurately average the growth rate of the 3-D perturbations over the statistics of the turbulent 2-D base flow. We leverage the capabilities of modern graphics processing units to achieve this task, which allows us to investigate the parameter space up to $Re = 10^5$. At the Reynolds numbers typical of 3-D direct numerical simulations and laboratory experiments, $Re \in [10^2, 5 \times 10^3]$, the turbulent 2-D flow becomes unstable to 3-D motion through a centrifugal-type instability. However, at even higher Reynolds numbers, another instability takes over. A candidate mechanism for the latter instability is the parametric excitation of inertial waves by the modulated 2-D flow, a phenomenon that we illustrate with an oscillatory 2-D Kolmogorov flow.

Key words: rotating turbulence, geostrophic turbulence

1. Introduction

Global rotation tends to make turbulent flows two-dimensional (2-D) and invariant along the rotation axis. This result is often referred to as the Taylor–Proudman theorem, which states that slowly evolving large-scale rapidly rotating flows organise into Taylor columns, invariant along the rotation axis (the vertical axis thereafter). However, in most numerical and experimental studies of rapidly rotating turbulence, these large-scale columns coexist

† Email address for correspondence: s.kannabiran@gmail.com

© The Author(s), 2020. Published by Cambridge University Press

https://doi.org/10.1017/jfm.2020.541 Published online by Cambridge University Press

with erratic three-dimensional (3-D) small-scale motion (Bartello, Métais & Lesieur 1994; Yeung & Zhou 1998; Smith & Waleffe 1999; Chen *et al.* 2005; Morize & Moisy 2006; Staplehurst, Davidson & Dalziel 2008; Thiele & Müller 2009; Moisy *et al.* 2011; Yarom, Vardi & Sharon 2013; Gallet *et al.* 2014; Yokoyama & Takaoka 2017; Seshasayanan & Alexakis 2018). Although the latter contain typically less kinetic energy than the large-scale columns, they need to be precisely characterised, because they are responsible for the efficient 3-D dissipation of kinetic energy (Campagne *et al.* 2015). Indeed, at the theoretical level, the 3-D inertial waves have been shown to induce a forward wave turbulent cascade leading to 'anomalous' kinetic energy dissipation, i.e. a dissipated power independent of molecular viscosity (Galtier 2003; Bellet *et al.* 2006). On the one hand, wave turbulence provides the right framework to address the decay of rotating turbulence initialised with inertial waves only. On the other hand, forced rotating turbulence in a finite domain generically exhibits intense Taylor columns when global rotation is sufficiently fast, which challenges a description in terms of inertial waves only (even when energy is input into wave modes only (see Brunet, Gallet & Cortet 2020; Le Reun *et al.* 2020)).

We focus on such forced rotating turbulence in statistically steady state. Restricting attention to a steady body force at scale L, the goal is to characterise the turbulent flows arising at large Reynolds number $Re = UL/\nu$, where U is the root-mean-square (r.m.s.) flow velocity and ν is the kinematic viscosity, and low Rossby number $Ro = U/2\Omega L$, where Ω denotes the global rotation rate. Two situations emerge depending on the spatial structure of the body force:

(i) When the body force is 3-D and directly drives some vertically dependent flow structures, it was shown by Alexakis (2015) that the statistically steady state never corresponds to a rapidly rotating turbulent flow with both $Re \gg 1$ and $Ro \ll 1$. The reason is that the r.m.s. velocity U is an emergent quantity that cannot be specified at the outset of a numerical simulation. In (non-turbulent) flows characterised by $Re \sim 1$, the flow can achieve arbitrarily low Ro provided the global rotation is fast enough. However, for turbulent flows with $Re \gg 1$, the r.m.s. velocity saturates at a value $U \sim \Omega L$, such that the Rossby number approaches unity.

(ii) By contrast, it is only when the body force is invariant along the rotation axis that one can reach simultaneously $Re \gg 1$ and $Ro \ll 1$, a regime that we refer to as rapidly rotating turbulence.

For the latter situation, one can prove that the flow becomes exactly 2-D when the Rossby number is reduced at fixed (but arbitrarily large) Reynolds number and fixed aspect ratio of the fluid domain, using rigorous upper bound theory. This has important consequences for the energy dissipation rate of rapidly rotating turbulent flows: the anomalous dissipation associated with the forward energy cascade of 3-D turbulence is replaced by the laminar-like viscous dissipation of the domain-scale velocity structures that arise from the 2-D inverse energy cascade (Alexakis & Doering 2006; van Bokhoven *et al.* 2009; Campagne *et al.* 2014; Deusebio *et al.* 2014; Campagne *et al.* 2016; Buzzicotti *et al.* 2018; van Kan & Alexakis 2020; Pestana & Hickel 2019). Mapping the energy dissipation rate of rotating turbulence in parameter space requires determination of the transition between exactly 2-D and partially 3-D rapidly rotating flows. Indeed, the mathematical results in Gallet (2015) only provide a lower bound on the critical Rossby number $Ro_c(Re)$ below which the flow becomes purely 2-D. The bound typically scales as Re^{-6} with logarithmic corrections, i.e. we are only able to prove that the flow becomes exactly 2-D for extremely low Rossby numbers. However, one should keep in mind that

https://doi.org/10.1017/jfm.2020.541 Published online by Cambridge University Press

this Re^{-6} scaling behaviour is only a limitation of the bounding method, not a property of the true threshold $Ro_c(Re)$: we establish in the following that $Ro_c(Re)$ is in fact much greater than Re^{-6}, so that exact two-dimensionalisation takes place over a signification region of parameter space.

The very existence of a clear-cut transition between exactly 2-D and partially 3-D flows suggests an alternative approach to the study of rapidly rotating turbulence: instead of running costly 3-D direct numerical simulations (DNS) at large Reynolds number and ever lower Rossby number, in the present study we start from high Re and very low Ro, where we know the flow is 2-D, and investigate the appearance of three-dimensionality as we increase Ro. The goal is to determine the boundary $Ro_c(Re)$ in parameter space between exactly 2-D flows and partially 3-D ones through linear stability analysis. The challenge is that the base state of this linear stability analysis is a body-forced turbulent 2-D flow. Because of the inverse energy cascade, such flows typically achieve a statistically steady state after a long transient, the duration of which scales with the viscous time scale L^2/ν. For a given Reynolds number $Re \gg 1$, one typically needs to integrate the 2-D equations for a number Re of large-scale eddy turnover times. Once the statistically steady 2-D base state is reached, thousands of additional turnover times are needed to correctly sample the growth rate of the infinitesimal 3-D perturbations and conclude on the stability of the flow. We leverage the capabilities of modern graphics processing units (GPUs) to address this challenge: the linear stability problem for the 3-D perturbations is effectively 2-D and fits on the memory of a single GPU, which outperforms central processing units (CPUs) for the rapid computation of fast Fourier transforms. This enables us to investigate the 2-D to 3-D transition up to $Re = 10^5$, one to two orders of magnitude above the typical values reported in experimental and fully 3-D numerical studies.

2. Theoretical set-up

We consider the flow of a Newtonian fluid inside a parallelepiped domain $(x, y, z) \in [0, L] \times [0, L] \times [0, H]$, in a frame rotating at a rate $\Omega > 0$ around the vertical z axis. We focus on periodic boundary conditions in all three directions, although the results apply equally to a fluid layer of height $H/2$ with stress-free boundary conditions at the top and bottom. The flow is driven by a vertically invariant body force $\boldsymbol{f} = f_0 \sin(8\pi y/L)\boldsymbol{e}_x$, where $\boldsymbol{e}_x$ denotes the unit vector along x, and the velocity field $\boldsymbol{u}(x, y, z, t)$ satisfies the rotating Navier–Stokes equation

$$\partial_t \boldsymbol{u} + (\boldsymbol{u} \cdot \boldsymbol{\nabla})\boldsymbol{u} + 2\Omega\, \boldsymbol{e}_z \times \boldsymbol{u} = -\boldsymbol{\nabla} p + \nu \Delta \boldsymbol{u} + \boldsymbol{f}, \tag{2.1}$$

together with the incompressibility constraint $\boldsymbol{\nabla} \cdot \boldsymbol{u} = 0$. This equation admits some vertically invariant 2-D solutions, $\boldsymbol{u}_{2\text{-D}}(x, y, t)$, that satisfy the 2-D Navier–Stokes equation

$$\partial_t \boldsymbol{u}_{2\text{-D}} + (\boldsymbol{u}_{2\text{-D}} \cdot \boldsymbol{\nabla})\boldsymbol{u}_{2\text{-D}} = -\boldsymbol{\nabla} P + \nu \Delta \boldsymbol{u}_{2\text{-D}} + \boldsymbol{f}, \tag{2.2}$$

where the Coriolis force is absorbed by the pressure gradient. In a non-rotating system and at large Reynolds number, such 2-D solutions are unstable to 3-D perturbations and quickly evolve into fully 3-D turbulence.

However, rapid global rotation stabilises these 2-D solutions with respect to 3-D perturbations, even the turbulent ones: at large Reynolds number and very low Rossby number, the flow $\boldsymbol{u}_{2\text{-D}}(x, y, t)$ evolves in a complicated and chaotic fashion, but it remains invariant in the vertical direction. Such exact two-dimensionalisation of the flow only holds

https://doi.org/10.1017/jfm.2020.541 Published online by Cambridge University Press

up to a Reynolds-number-dependent and aspect-ratio-dependent critical Rossby number $Ro_c(Re, L/H)$ above which three-dimensionality spontaneously arises. To determine the precise threshold Ro_c, we consider the evolution of an infinitesimal 3-D perturbation to the 2-D turbulent base flow $\boldsymbol{u}_{2\text{-D}}(x, y, t)$. This 3-D perturbation satisfies the Navier–Stokes equation (2.1) linearised around $\boldsymbol{u}_{2\text{-D}}$. Because the latter is independent of z, the different vertical Fourier modes of the 3-D perturbation decouple at linear order. Without loss of generality, we can thus restrict attention to a 3-D perturbation consisting of a single vertical Fourier mode, $\hat{\boldsymbol{u}}_{3\text{-D}}(x, y, t)\, \mathrm{e}^{\mathrm{i}qz}$, where $\hat{\boldsymbol{u}}_{3\text{-D}}(x, y, t)$ is a complex-valued 3-D vector. The full velocity field is $\boldsymbol{u}(x, y, z, t) = \boldsymbol{u}_{2\text{-D}}(x, y, t) + \hat{\boldsymbol{u}}_{3\text{-D}}(x, y, t)\, \mathrm{e}^{\mathrm{i}qz} + \text{c.c.}$, where c.c. denotes the complex conjugate of the second term. Upon linearising the vorticity equation around the 2-D base flow, we obtain the evolution equation for the vorticity of the 3-D perturbation, $\hat{\boldsymbol{\omega}}_{3\text{-D}} = (\boldsymbol{\nabla}_\perp + \mathrm{i}q\boldsymbol{e}_z) \times \hat{\boldsymbol{u}}_{3\text{-D}}$:

$$\begin{aligned} \partial_t \hat{\boldsymbol{\omega}}_{3\text{-D}} = (\boldsymbol{\nabla}_\perp + \mathrm{i}q\boldsymbol{e}_z) \times [\boldsymbol{u}_{2\text{-D}} \times \hat{\boldsymbol{\omega}}_{3\text{-D}} + \hat{\boldsymbol{u}}_{3\text{-D}} \times (\omega_{2\text{-D}}\boldsymbol{e}_z)] \\ + 2\mathrm{i}q\Omega\, \hat{\boldsymbol{u}}_{3\text{-D}} + \nu(\nabla_\perp^2 - q^2)\hat{\boldsymbol{\omega}}_{3\text{-D}}, \end{aligned} \tag{2.3}$$

where $\boldsymbol{\nabla}_\perp = (\partial_x, \partial_y, 0)$ and $\omega_{2\text{-D}} = (\boldsymbol{\nabla}_\perp \times \boldsymbol{u}_{2\text{-D}}) \cdot \boldsymbol{e}_z$.

Linear stability analysis thus boils down to an effectively 2-D fluid problem governed by (2.2) and (2.3). However, the aspect ratio of the 3-D domain remains a key control parameter, as it restricts the acceptable values of the vertical wavenumber q entering these 2-D equations. Anticipating the results presented in figure 2, we observe that Ro_c is an increasing function of the vertical wavenumber $|q|$ throughout most of the parameter space. In other words, the most unstable mode corresponds to the gravest vertical wavenumber compatible with the vertical boundary conditions, $q = 2\pi/H$. Linear stability analysis for a low value of qL thus yields the threshold Rossby number for a deep domain, while linear stability analysis for a large value of qL yields the threshold Rossby number for a shallow domain, the dimensionless vertical wavenumber and the aspect ratio being related by $qL = 2\pi L/H$. In the following, we thus refer to the threshold Rossby number computed for low (respectively large) values of qL as the onset of 3-D motion in deep (respectively shallow) fluid layers.

The stability analysis consists of two steps. First, we integrate (2.2) until the 2-D turbulent flow reaches a statistically steady state, which constitutes the base state of the linear stability analysis. This base flow is independent of the global rotation rate Ω, which does not appear in (2.2). Secondly, we introduce the 3-D perturbation by solving simultaneously (2.2) and (2.3).

We compute the r.m.s. velocity from the statistically steady 2-D base flow, $U = \langle \boldsymbol{u}_{2\text{-D}}^2 \rangle_{\boldsymbol{x},t}^{1/2}$, where $\langle \cdot \rangle_{\boldsymbol{x},t}$ denotes an average over space and time. Even though U is an emergent quantity – as opposed to a true control parameter of (2.2) – we build the Reynolds number Re and Rossby number Ro with this r.m.s. velocity to facilitate comparison with other experimental and numerical set-ups. The relation between Re and the forcing-based Grashof number associated with (2.2) is provided in the appendix. The problem thus involves three dimensionless parameters: the Reynolds and Rossby numbers defined above, and the aspect ratio of the fluid domain through the dimensionless vertical wavenumber qL. A typical set of numerical runs consists in holding Re and qL fixed, and sweeping over the values of Ro by changing the rotation rate Ω. The corresponding time series of the kinetic energy of the 3-D perturbation, $E_{3\text{-D}}(t) = \langle |\hat{\boldsymbol{u}}_{3\text{-D}}|^2 \rangle_{\boldsymbol{x}}$, are displayed in figure 1 for such a set of runs. For low Rossby number (large rotation rate), the 3-D kinetic energy decays monotonically in time: the 2-D turbulent base flow is stable with respect to

https://doi.org/10.1017/jfm.2020.541 Published online by Cambridge University Press

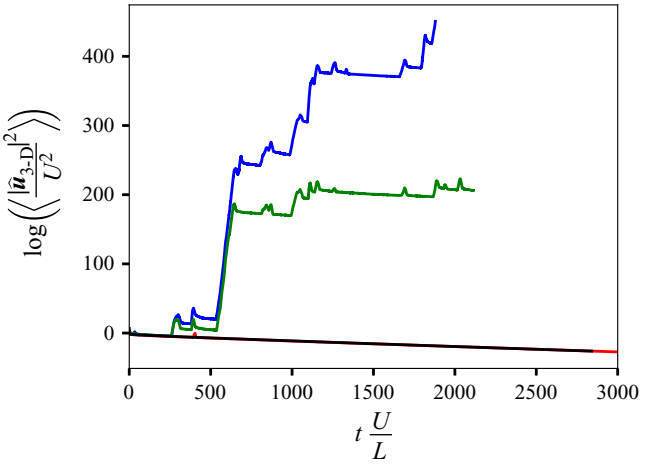


FIGURE 1. Time series of the kinetic energy of the 3-D perturbation, for fixed Reynolds number $Re = 9.3 \times 10^4$ and aspect ratio $qL = 6\pi$. The Rossby number increases from bottom to top: $Ro = 3.7 \times 10^{-3}$ (black), 4.9×10^{-3} (red), 7.4×10^{-3} (green) and 9.8×10^{-3} (blue), respectively. The first two time series correspond to stable situations, while the 3-D perturbation grows exponentially for the two highest values of Ro.

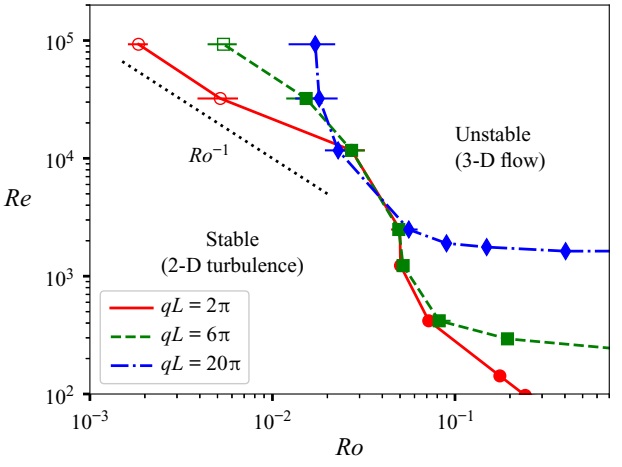


FIGURE 2. Threshold for instability to 3-D perturbations in the (Ro, Re) plane, for three values of the aspect ratio. Full symbols with $Ro \in [0.015, 0.03]$ correspond to a centrifugal-type instability. The open symbols at lower Ro depart from this behaviour, and display the characteristics of the parametric excitation of inertial waves.

3-D perturbations. By contrast, for larger Rossby number, the 3-D kinetic energy grows rapidly, indicating an instability. The growth rate of the 3-D kinetic energy displays a strongly intermittent behaviour, associated with the turbulent dynamics of the background 2-D flow.

Through long numerical integrations we infer the average growth rate, $\gamma = \langle (\mathrm{d}/\mathrm{d}t) \log E_{3\text{-D}} \rangle_t$, as a function of the Rossby number Ro. The threshold Rossby number $Ro_c(Re, qL)$ for the emergence of three-dimensionality is obtained when $\gamma = 0$. We determine $Ro_c(Re, qL)$ by repeating similar sets of numerical runs for various values of Re and qL

https://doi.org/10.1017/jfm.2020.541 Published online by Cambridge University Press

and show it in figure 2. The boundary clearly separates the low-Ro region of parameter space, where the system has 2-D flow attractors, from the large-Ro region, where the flow becomes 3-D. It is worth stressing the fact that Ro_c is much larger than the conservative lower bound computed in Gallet (2015): the threshold lies in a region of parameter space accessible to DNS (Godeferd & Lollini 1999; Mininni, Alexakis & Pouquet 2009; Mininni & Pouquet 2010) and laboratory experiments (Hopfinger, Browand & Gagne 1982; Dickinson & Long 1983; Morize & Moisy 2006; Gallet *et al.* 2014; Yarom & Sharon 2014), which typically reach $Re \leq 3000$ and $Ro \in [10^{-2}, 1]$. However, the integration of the quasi-2-D equations on GPUs allows us to extend this boundary to more extreme values of the dimensionless parameters, all the way to $Re \simeq 10^5$ and $Ro \simeq 2 \times 10^{-3}$.

The location of the boundary depends on the aspect ratio qL: for a shallow fluid layer with $qL = 20\pi$, Ro_c seems to asymptote to a Re-independent value at large Re, at least up to $Re = 10^5$. By contrast, for deeper fluid layers (lower values of qL), Ro_c does depend on Re at large Reynolds number, with the approximate scaling behaviour $Ro_c \sim Re^{-1}$, shown as a dashed line in figure 2. The instability arises over a turbulent base state, a situation less documented than standard instabilities arising over steady or periodic base flows. To gain intuition into the instability process, we thus pursue two approaches. First, we compare the present instability to known instabilities of steady vortices in rotating flows, namely the centrifugal and elliptical instabilities. Secondly, we discuss the decomposition of the low-Ro 3-D perturbation into inertial waves, the instabilities of which can be investigated through a perturbative expansion in Rossby number.

3. Centrifugal instability

For the shallowest fluid domain considered in figure 2 $qL = 20\pi$, the 3-D instability exhibits many features of the centrifugal instability. First, we observe that the unstable mode develops only inside anticyclones, an example being provided in figure 3(*a*,*d*). Secondly, the inviscid Rayleigh criterion for the centrifugal instability of an axisymmetric vortex is that the quantity $\phi(r) = 2[V(r)/r + \Omega][\omega_{2\text{-D}}(r) + 2\Omega]$ be negative for some value of r, where $V(r)$ and $\omega_{2\text{-D}}(r)$ are the azimuthal velocity profile and the vorticity profile, respectively (Kloosterziel & Van Heijst 1991). For a given radial structure of the anticyclone, this instability criterion yields $\omega(r = 0) + \mathcal{C}\Omega < 0$, where the first term is the (negative) vorticity at the vortex centre, and $\mathcal{C} > 0$ is a dimensionless constant that depends on the shape of the anticyclone (Sipp, Lauga & Jacquin 1999; Sipp & Jacquin 2000). As a proxy to the Rayleigh criterion, we have computed the quantity $\mathcal{R}(t) = [\overline{\min_x(\omega_{2\text{-D}})} + 2\Omega]/2\Omega$, where the overline denotes a smoothing over one turnover time L/U. In figure 4, we represent a scatter plot of the (smoothed) instantaneous growth rate $\overline{(\mathrm{d}/\mathrm{d}t)(\log E_{3\text{-D}})}$ as a function of $\mathcal{R}(t)$. The two quantities are strongly correlated, the growth rate being positive whenever Rayleigh's instability criterion is satisfied, i.e. when $\mathcal{R}(t) \lesssim 0$. This is another indication that the instability arising in the present system is of centrifugal type.

Finally, rigorous upper bound theory indicates that the time average of the minimum 2-D vorticity scales with the large-scale turnover time, $|\langle \min_x(\omega_{2\text{-D}})\rangle_t| \lesssim U/L$ up to logarithmic terms (see appendix A.3 in Gallet 2015). This is an indication that $\overline{\min_x(\omega_{2\text{-D}})}$ scales as U/L, so that the generalised Rayleigh criterion yields $Ro \leq$ const.: at low viscosity (large Reynolds number), we expect the centrifugal instability to arise above a Re-independent threshold Rossby number. The shallow-layer $qL = 20\pi$ data in figure 2 indeed asymptote to a Re-independent threshold Rossby number at large Re.

https://doi.org/10.1017/jfm.2020.541 Published online by Cambridge University Press

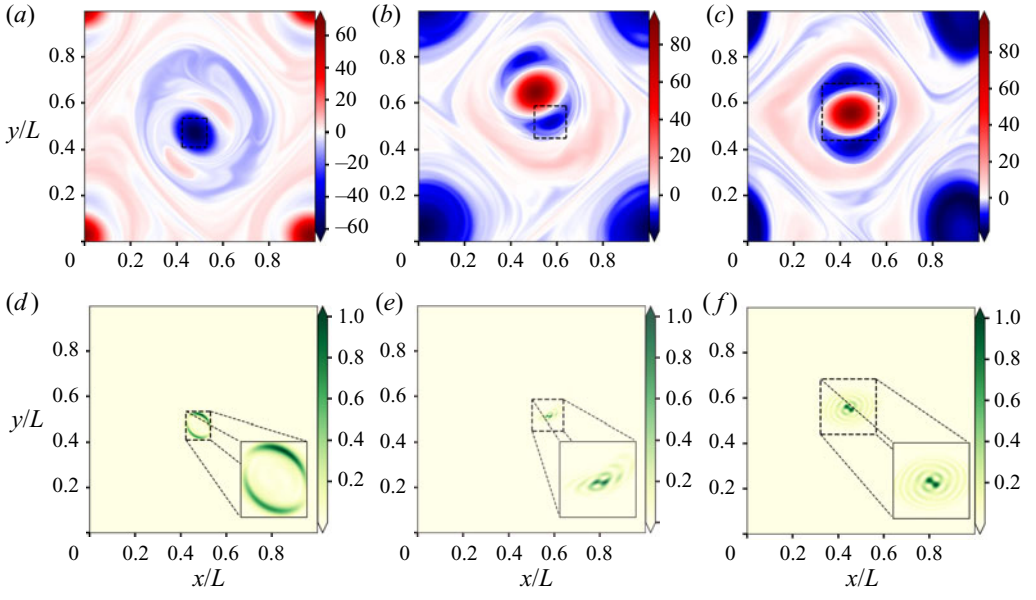


FIGURE 3. Unstable mode near threshold: (*a–c*) normalised vorticity $\omega_{2\text{-D}}(L/U)$ of the 2-D turbulent base flow and (*d–f*) corresponding unstable three-dimensional perturbation; (*a,d*) $Re = 9.3 \times 10^4$, $qL = 20\pi$, $Ro = 2.0 \times 10^{-2}$, (*b,e*) $Re = 9.3 \times 10^4$, $qL = 6\pi$, $Ro = 7.4 \times 10^{-3}$ and (*c,f*) $Re = 9.3 \times 10^4$, $qL = 2\pi$, $Ro = 2.7 \times 10^{-3}$.

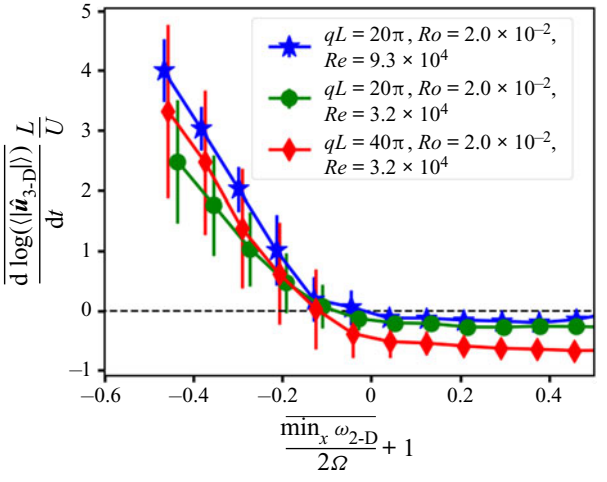


FIGURE 4. Scatter plot of the smoothed growth rate versus the Rayleigh-like parameter $\mathcal{R}(t) = \overline{\min_x(\omega_{2\text{-D}})}/2\Omega + 1$. The symbols correspond to the mean value in each horizontal bin and the vertical bars show the standard deviation. The strong correlation between the two quantities is characteristic of a centrifugal instability developing inside anticyclones when $\mathcal{R}(t) \lesssim 0$.

A similar correlation between the Rayleigh criterion $\mathcal{R}(t)$ and the growth rate was observed for all the filled symbols in figure 2 with $Ro \lesssim 0.1$, which indicates that the corresponding instability is of centrifugal type. However, for large Reynolds number and

https://doi.org/10.1017/jfm.2020.541 Published online by Cambridge University Press

lower values of the vertical wavenumber, $qL = 6\pi$ or $qL = 2\pi$ (i.e. for deeper fluid layers), we observed no clear correlations between $\mathcal{R}(t)$ and the growth rate: these are the open symbols in figure 2. These data points also depart from the $Ro_c = \text{const.}$ asymptote of the shallow layer $qL = 20\pi$, which is additional evidence that they do not correspond to a centrifugal instability.

4. Three-dimensionality in deeper fluid layers

For lower values of qL (deeper fluid layers) and large Reynolds number, the threshold to three-dimensionality departs from the $Ro = \text{const.}$ centrifugal asymptote (see figure 2). The deeper the layer, the lower the value qL of the gravest vertical mode, and the sooner the threshold departs from the asymptote as Re increases. We conjecture that the $qL = 20\pi$ threshold would probably also depart from the centrifugal asymptote if we could investigate even higher Reynolds numbers. There is thus another instability at play in deep domains and at large Reynolds number. To characterise the corresponding unstable modes, in the second and third columns of figure 3 we provide snapshots of the 2-D base flow and 3-D perturbation, during a phase of rapid growth of the latter. A first difference with the centrifugal instability is that the unstable mode can develop inside the elliptical core of both cyclones (figure 3*b*,*e*) and anticyclones (figure 3*c*,*f*). This points towards the elliptical instability as a potential candidate for this large-Re instability.

However, at least two arguments seem to challenge this interpretation. First, we played the – arguably artificial – game of replacing the 2-D turbulent base flow by a steady flow that corresponds to either figure 3(*b*) or 3(*c*) (i.e. we freeze the 2-D base flow). We probed the stability of the frozen flow over a range of Rossby numbers that extends up to twice the threshold Rossby number of instability of the time-dependent flow. Surprisingly, we observed that such artificial steady flows do not lead to an instability over that range of Rossby numbers. The unavoidable conclusion is that the time dependence of the base flow plays a central role in the instability mechanism, which thus differs from the simple elliptical instability of a steady vortex. Secondly, theoretical predictions based on weak-ellipticity expansions lead to a threshold for instability of the form $Re \sim Ro^{-2}$ (Le Dizes & Eloy 1999; Le Dizes 2000), while our data points indicate a scaling law closer to $Re \sim Ro^{-1}$ for the 2-D/3-D threshold at high Re in deep domains, albeit in a moderate parameter range (see figure 2 for $qL = 6\pi$ and $qL = 2\pi$).

Because the high-Re deep-domain instability arises at low Rossby number, we can address it through a standard low-Ro inertial-wave expansion of the 3-D perturbation. In this framework, the 2-D base flow and the 3-D perturbation are decomposed onto a helical basis of inertial waves, with slowly varying amplitudes. These wave amplitudes evolve primarily through resonant triadic interactions. However, these interactions do not transfer energy between the 3-D waves and the 2-D base flow, and therefore the 3-D instability cannot arise from resonant triadic interactions (Greenspan 1968; Smith & Waleffe 1999; Chen *et al.* 2005). In some sense, this is the reason behind the existence of exact two-dimensionalisation: these instabilities, which would lead to a constant threshold Reynolds number Re_c (set by the balance between an inviscid growth rate $\gamma \sim U/L$ and the viscous damping rate ν/L^2) cannot arise over a purely 2-D base flow. Instead, one needs to go to the next order in Rossby number to uncover mechanisms that do transfer energy between the 2-D flow and the 3-D perturbations. At this order, quasi-resonant triads and resonant quartets of inertial waves were recently highlighted as important instability mechanisms to induce 2-D motion from an inertial-wave base flow (Kerswell 1999;

https://doi.org/10.1017/jfm.2020.541 Published online by Cambridge University Press

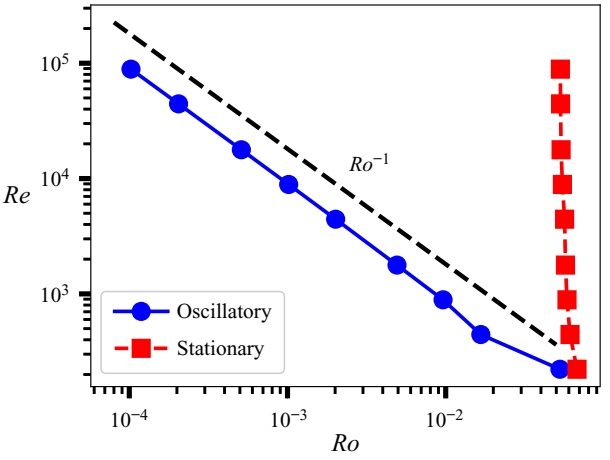


FIGURE 5. Threshold of instability to 3-D perturbations in the (Ro, Re) plane for an oscillatory Kolmogorov flow (blue circles) and a steady Kolmogorov flow (red squares). While the steady Kolmogorov flow has a $Ro \simeq$ const. instability threshold, the oscillatory Kolmogorov flow is much more unstable, with a threshold Reynolds number that scales as Ro^{-1} (dashed line).

Smith & Waleffe 1999; Le Reun 2019; Le Reun, Favier & Le Bars 2019; Brunet *et al.* 2020; Le Reun *et al.* 2020).

We argue that the opposite mechanisms can arise in the present system: 3-D inertial waves can arise spontaneously over a 2-D base flow, either through resonant quartets of inertial waves, or through the parametric excitation of inertial waves by the time-dependent 2-D flow. Both mechanisms would lead to an inviscid growth rate $\gamma \sim Ro\, U/L$: at threshold, the latter balances the viscous damping rate ν/L^2, which leads to a threshold $Re \sim Ro^{-1}$ in parameter space. The parametric excitation of inertial waves by the time-dependent 2-D flow is a particularly appealing mechanism, as it provides an explanation for both the $Re \sim Ro^{-1}$ scaling behaviour and the key role of the time dependence of the base flow. A simple illustration of this mechanism is provided by the oscillatory Kolmogorov flow: instead of the intricate 2-D turbulent base flow, consider the simpler flow $\boldsymbol{u}_{2\text{-D}} = 2U \sin(4\pi y/L) \cos(4\pi Ut/L)\boldsymbol{e}_x$ as a model of large-scale flow structures of typical velocity U evolving with the eddy turnover time L/U. We determine the threshold for the growth of 3-D perturbations around this 2-D base flow using a numerical code based on Floquet theory in time. As shown in figure 5 for $qL = 2\pi$, the threshold of the corresponding parametric instability scales as $Re \sim Ro^{-1}$ (blue circles). By contrast, the steady version of this Kolmogorov flow, $\boldsymbol{u}_{2\text{-D}} = \sqrt{2}U \sin(4\pi y/L)\boldsymbol{e}_x$, yields an instability threshold $Ro \simeq$ const. (red squares), reminiscent of the centrifugal asymptote in figure 2. Indeed, for such a parallel flow the streamlines have an infinite radius of curvature, and the ϕ centrifugal-instability criterion above reduces to the existence of a point in the flow where $\omega_{2\text{-D}} \leq -2\Omega$. This criterion yields a threshold Rossby number $Ro_c = 1/(4\pi\sqrt{2}) \simeq 0.0563$ for the steady Kolmogorov flow, in excellent agreement with the numerical value (see figure 5).

The stark contrast between the instability thresholds of the steady and oscillatory Kolmogorov flows in figure 5 illustrates once again that the time dependence of the 2-D base flow is a key ingredient for instability to 3-D perturbations at high Reynolds number and low Rossby number.

https://doi.org/10.1017/jfm.2020.541 Published online by Cambridge University Press

5. Discussion

We have investigated the onset of three-dimensionality in rapidly rotating turbulent flows using the capabilities of modern GPUs. Interestingly, the threshold between exactly 2-D and partially 3-D flows crosses the region of parameter space that is accessible to laboratory experiments and fully 3-D DNS. In this region of parameter space, we have provided evidence that three-dimensionality arises through the centrifugal destabilisation of anticyclones. The corresponding threshold Rossby number depends only weakly on the Reynolds number for large enough Re. However, our approach also allowed us to reach a region of parameter space that goes beyond the parameter range of state-of-the-art experiments and DNS, up to $Re = 10^5$ and $Ro = 2 \times 10^{-3}$ simultaneously. For such extreme parameter regimes, the threshold between 2-D and 3-D flows scales as $Re \sim Ro^{-1}$, and the time dependence of the base flow appears as a crucial ingredient of the instability process. We proposed the parametric amplification of inertial waves by the fluctuating 2-D turbulent flow as a candidate mechanism for this instability, which we exemplified through the stability analysis of the rapidly rotating oscillatory Kolmogorov flow. Whether and how this instability is connected to standard forms of the elliptical instability remains to be investigated. The scaling $Re \sim Ro^{-1}$ for the instability threshold is yet another confirmation that the limits $Re \to \infty$ and $Ro \to 0$ do not commute: the end state of rapidly rotating turbulence depends very much on the distinguished limit considered when sending Re to infinity and Ro to zero (Alexakis 2015; Gallet 2015; Le Reun 2019).

While this study is motivated primarily by theoretical fluid dynamics, some connection can be made to the dynamics of natural flows. Very much like rotating turbulence can be decomposed into a 2-D slow manifold coexisting with 3-D waves, rotating stratified oceanic and atmospheric flows can be decomposed into balanced motion – the quasi-geostrophic slow manifold – and waves. In both cases the slow manifold leads to an inverse energy cascade, with energy condensing into domain-scale structures in the absence of large-scale damping, and in both cases the waves can induce a 'wave-turbulent' forward energy cascade. Because such condensation of kinetic energy at the basin scale is absent from oceanic data, it has been hypothesised that part of the balanced energy may be transferred to wave-like motion and cascaded to small scales, a phenomenon coined 'loss of balance' (Vanneste 2013; Rocha, Wagner & Young 2018). In the simpler context of rapidly rotating unstratified turbulence, the slow manifold consists of 2-D flows, and loss of balance corresponds to the emergence of 3-D waves. Our study thus highlights basic instability mechanisms leading to spontaneous loss of balance in a rapidly rotating unstratified turbulent flow. It provides the region of parameter space where 3-D structures develop, shedding light on the possible emergence of a forward energy cascade as the Rossby number increases.

We stress the fact that the present linear stability analysis only provides sufficient conditions for the emergence of 3-D structures. For Rossby numbers lower than Ro_c, we cannot rule out the emergence of three-dimensionality through finite-amplitude instabilities (FAIs). In other words, below $Ro_c(Re)$ we know that the system possesses a 2-D flow attractor, but this attractor may coexist in phase space with a fully 3-D flow attractor (see e.g. Yokoyama & Takaoka (2017) for the coexistence of a quasi-2-D attractor and a strongly 3-D one). The statistically steady state realised by the system would then depend on the initial condition. As shown in Gallet (2015), however, there exists a value $Ro_{abs}(Re)$ of the Rossby number below which such FAIs are ruled out: for $Ro \leq Ro_{abs}(Re)$, the 2-D flow is absolutely stable to 3-D perturbations and the system ends up in the 2-D flow attractor regardless of the initial condition. If $Ro_{abs}(Re) < Ro_c(Re)$, then FAIs can

https://doi.org/10.1017/jfm.2020.541 Published online by Cambridge University Press

Re	qL	Resolution (N_x, N_y)	$\mathrm{d}t\dfrac{U}{L}$
$\leq 5 \times 10^2$	$[2\pi, 6\pi, 20\pi]$	256×256	$[3 \times 10^{-4}, 5 \times 10^{-4}]$
$[1, 2 \times 10^3, 2.5 \times 10^3]$	$[2\pi, 6\pi, 20\pi]$	384×384	2×10^{-4}
1.2×10^4	$[2\pi, 6\pi, 20\pi]$	512×512	10^{-4}
3.2×10^4	$[2\pi, 6\pi, 20\pi]$	1024×1024	7×10^{-5}
9.3×10^4	$[2\pi, 6\pi, 20\pi]$	1536×1536	4×10^{-5}

TABLE 1. Resolution (N_x, N_y) and average (adaptive) time step $\mathrm{d}t(U/L)$ for the values of the Reynolds number considered in this study. The simulations are run for a large number of time steps, of the order of $Re\,L/(U\,\mathrm{d}t)$.

arise for $Ro \in [Ro_{abs}(Re), Ro_c(Re)]$, depending on the initial condition. If $Ro_{abs}(Re) = Ro_c(Re)$, FAIs are ruled out. Again, the determination of $Ro_{abs}(Re)$ through fully 3-D DNS remains prohibitively expensive at large Re and low Ro. Instead, the existence of FAIs, as well as whether and when a forward energy cascade develops, could be investigated through nonlinear extensions of this work: one could design a weakly nonlinear model by keeping only the first unstable vertically dependent mode and its feedback onto the 2-D base flow, in the spirit of Benavides & Alexakis (2017) and Seshasayanan, Gallet & Alexakis (2017). For physical systems that are amenable to 3-D DNS in extreme parameter regimes, models of this kind have predictive skills when compared to 3-D DNS, at least at a qualitative level (van Kan & Alexakis 2019). For the problem at stake, such a model may capture the emergence of a forward energy cascade as Ro increases (Alexakis & Biferale 2018), thus providing direct information on the region of parameter space where rapidly rotating turbulence displays an 'anomalous' or fully turbulent energy dissipation rate, independent of molecular viscosity.

Acknowledgements

We thank S. Le Dizès, S. Benavides and A. Alexakis for insightful discussions. This work is supported by the European Research Council under grant agreement 757239.

Declaration of interests

The authors report no conflicts of interest.

Appendix. Numerical methods

The numerical simulations are performed using standard pseudo-spectral methods, with dealiasing using the two-thirds rule. The fields are decomposed into a Fourier–Fourier basis in spectral space and discretised on a (N_x, N_y) grid in the x and y directions of the physical space. Time stepping is performed using a standard four-step third-order Runge–Kutta scheme. The adaptive time step $\mathrm{d}t$ satisfies a Courant–Friedrichs–Lewy (CFL) condition constructed from both advective and rotation time scales. The spatial resolutions and the average time step are given in table 1. The simulations are run for a number of time steps of the order of $Re\,L/(U\,\mathrm{d}t)$.

https://doi.org/10.1017/jfm.2020.541 Published online by Cambridge University Press

Simulations of the 2-D Navier–Stokes equations (2.2) are performed until the flow reaches a statistically steady state, which constitutes the base flow of the present linear stability analysis. The Reynolds and Rossby numbers are built using the r.m.s. velocity U of this 2-D base flow. The control parameter of the 2-D Navier–Stokes equation (2.2) is the Grashof number $Gr = f_0^{1/2} L^{3/2}/\nu$, while the r.m.s. velocity U is an emergent quantity. For low Grashof number, U is given by the laminar balance between the viscous and forcing terms, $U/\sqrt{f_0 L} \sim Gr$. For larger Grashof number, $Gr \gtrsim 500$, the r.m.s. velocity obeys the approximate scaling law $U/\sqrt{f_0 L} \simeq 6.0 \times 10^{-3}\, Gr^{1/2}$ with 20 % accuracy.

References

Alexakis, A. 2015 Rotating Taylor–Green flow. *J. Fluid Mech.* **769**, 46–78.

Alexakis, A. & Biferale, L. 2018 Cascades and transitions in turbulent flows. *Phys. Rep.* **767–769**, 1–101.

Alexakis, A. & Doering, C. R. 2006 Energy and enstrophy dissipation in steady state 2D turbulence. *Phys. Lett.* A **359** (6), 652–657.

Bartello, P., Métais, O. & Lesieur, M. 1994 Coherent structures in rotating three-dimensional turbulence. *J. Fluid Mech.* **273**, 1–29.

Bellet, F., Godeferd, F. S., Scott, J. F. & Cambon, C. 2006 Wave turbulence in rapidly rotating flows. *J. Fluid Mech.* **562**, 83–121.

Benavides, S. J. & Alexakis, A. 2017 Critical transitions in thin layer turbulence. *J. Fluid Mech.* **822**, 364–385.

van Bokhoven, L. J. A., Clercx, H. J. H., van Heijst, G. J. F. & Trieling, R. R. 2009 Experiments on rapidly rotating turbulent flows. *Phys. Fluids* **21** (9), 096601.

Brunet, M., Gallet, B. & Cortet, P.-P. 2020 Shortcut to geostrophy in wave-driven rotating turbulence: the quartetic instability. *Phys. Rev. Lett.* **124** (12), 124501.

Buzzicotti, M., Aluie, H., Biferale, L. & Linkmann, M. 2018 Energy transfer in turbulence under rotation. *Phys. Rev. Fluids* **3** (3), 034802.

Campagne, A., Gallet, B., Moisy, F. & Cortet, P.-P. 2014 Direct and inverse energy cascades in a forced rotating turbulence experiment. *Phys. Fluids* **26** (12), 125112.

Campagne, A., Gallet, B., Moisy, F. & Cortet, P.-P. 2015 Disentangling inertial waves from eddy turbulence in a forced rotating-turbulence experiment. *Phys. Rev.* E **91** (4), 043016.

Campagne, A., Machicoane, N., Gallet, B., Cortet, P.-P. & Moisy, F. 2016 Turbulent drag in a rotating frame. *J. Fluid Mech.* **794**, R5.

Chen, Q., Chen, S., Eyink, G. L. & Holm, D. D. 2005 Resonant interactions in rotating homogeneous three-dimensional turbulence. *J. Fluid Mech.* **542**, 139–164.

Deusebio, E., Boffetta, G., Lindborg, E. & Musacchio, S. 2014 Dimensional transition in rotating turbulence. *Phys. Rev.* E **90** (2), 023005.

Dickinson, S. C. & Long, R. R. 1983 Oscillating-grid turbulence including effects of rotation. *J. Fluid Mech.* **126**, 315–333.

Gallet, B. 2015 Exact two-dimensionalization of rapidly rotating large-Reynolds-number flows. *J. Fluid Mech.* **783**, 412–447.

Gallet, B., Campagne, A., Cortet, P-P & Moisy, F. 2014 Scale-dependent cyclone-anticyclone asymmetry in a forced rotating turbulence experiment. *Phys. Fluids* **26** (3), 035108.

Galtier, S. 2003 Weak inertial-wave turbulence theory. *Phys. Rev.* E **68** (1), 015301.

Godeferd, F. S. & Lollini, L. 1999 Direct numerical simulations of turbulence with confinement and rotation. *J. Fluid Mech.* **393**, 257–308.

Greenspan, H. P. 1968 *The Theory of Rotating Fluids*. Cambridge University Press.

Hopfinger, E. J., Browand, F. K. & Gagne, Y. 1982 Turbulence and waves in a rotating tank. *J. Fluid Mech.* **125**, 505–534.

van Kan, A. & Alexakis, A. 2019 Condensates in thin-layer turbulence. *J. Fluid Mech.* **864**, 490–518.

https://doi.org/10.1017/jfm.2020.541 Published online by Cambridge University Press

VAN KAN, A. & ALEXAKIS, A. 2020 Critical transition in fast-rotating turbulence within highly elongated domains. *J. Fluid Mech.* **899**, A33.

KERSWELL, R. R. 1999 Secondary instabilities in rapidly rotating fluids: inertial wave breakdown. *J. Fluid Mech.* **382**, 283–306.

KLOOSTERZIEL, R. C. & VAN HEIJST, G. J. F. 1991 An experimental study of unstable barotropic vortices in a rotating fluid. *J. Fluid Mech.* **223**, 1–24.

LE DIZES, S. 2000 Three-dimensional instability of a multipolar vortex in a rotating flow. *Phys. Fluids* **12** (11), 2762–2774.

LE DIZES, S. & ELOY, C. 1999 Short-wavelength instability of a vortex in a multipolar strain field. *Phys. Fluids* **11** (2), 500–502.

LE REUN, T. 2019 Régimes asymptotiques des écoulements en rotation excités par forçage mécanique dans les noyaux planétaires: saturation turbulente et organisation à grande échelle. Thèse de doctorat, Aix-Marseille University.

LE REUN, T., FAVIER, B. & LE BARS, M. 2019 Experimental study of the nonlinear saturation of the elliptical instability: inertial wave turbulence versus geostrophic turbulence. *J. Fluid Mech.* **879**, 296–326.

LE REUN, T., GALLET, B., FAVIER, B. & LE BARS, M. 2020 Near-resonant instability of geostrophic modes: beyond Greenspan's theorem. *J. Fluid Mech.* **900**, R2.

MININNI, P. D., ALEXAKIS, A. & POUQUET, A. 2009 Scale interactions and scaling laws in rotating flows at moderate Rossby numbers and large Reynolds numbers. *Phys. Fluids* **21** (1), 015108.

MININNI, P. D. & POUQUET, A. 2010 Rotating helical turbulence. Part 1. Global evolution and spectral behavior. *Phys. Fluids* **22** (3), 035105.

MOISY, F, MORIZE, C, RABAUD, M & SOMMERIA, J 2011 Decay laws, anisotropy and cyclone–anticyclone asymmetry in decaying rotating turbulence. *J. Fluid Mech.* **666**, 5–35.

MORIZE, C. & MOISY, F. 2006 Energy decay of rotating turbulence with confinement effects. *Phys. Fluids* **18** (6), 065107.

PESTANA, T. & HICKEL, S. 2019 Regime transition in the energy cascade of rotating turbulence. *Phys. Rev.* E **99** (5), 053103.

ROCHA, C. B., WAGNER, G. L. & YOUNG, W. R. 2018 Stimulated generation: extraction of energy from balanced flow by near-inertial waves. *J. Fluid Mech.* **847**, 417–451.

SESHASAYANAN, K. & ALEXAKIS, A. 2018 Condensates in rotating turbulent flows. *J. Fluid Mech.* **841**, 434–462.

SESHASAYANAN, K., GALLET, B. & ALEXAKIS, A. 2017 Transition to turbulent dynamo saturation. *Phys. Rev. Lett.* **119** (20), 204503.

SIPP, D. & JACQUIN, L. 2000 Three-dimensional centrifugal-type instabilities of two-dimensional flows in rotating systems. *Phys. Fluids* **12** (7), 1740–1748.

SIPP, D., LAUGA, E. & JACQUIN, L. 1999 Vortices in rotating systems: centrifugal, elliptic and hyperbolic type instabilities. *Phys. Fluids* **11** (12), 3716–3728.

SMITH, L. M. & WALEFFE, F. 1999 Transfer of energy to two-dimensional large scales in forced, rotating three-dimensional turbulence. *Phys. Fluids* **11** (6), 1608–1622.

STAPLEHURST, P. J., DAVIDSON, P. A. & DALZIEL, S. B. 2008 Structure formation in homogeneous freely decaying rotating turbulence. *J. Fluid Mech.* **598**, 81–105.

THIELE, M. & MÜLLER, W.-C. 2009 Structure and decay of rotating homogeneous turbulence. *J. Fluid Mech.* **637**, 425–442.

VANNESTE, J. 2013 Balance and spontaneous wave generation in geophysical flows. *Annu. Rev. Fluid Mech.* **45** (1), 147–172.

YAROM, E. & SHARON, E. 2014 Experimental observation of steady inertial wave turbulence in deep rotating flows. *Nat. Phys.* **10**, 510–514.

YAROM, E., VARDI, Y. & SHARON, E. 2013 Experimental quantification of inverse energy cascade in deep rotating turbulence. *Phys. Fluids* **25** (8), 085105.

YEUNG, P. K. & ZHOU, Y. 1998 Numerical study of rotating turbulence with external forcing. *Phys. Fluids* **10** (11), 2895–2909.

YOKOYAMA, N. & TAKAOKA, M. 2017 Hysteretic transitions between quasi-two-dimensional flow and three-dimensional flow in forced rotating turbulence. *Phys. Rev. Fluids* **2** (9), 092602.

https://doi.org/10.1017/jfm.2020.541 Published online by Cambridge University Press